Bonding Patterns in a Strong 3c2e C−H···C Hydrogen Bond

Donald B. DuPré*

Department of Chemistry, University of Louisville, Louisville, Kentucky 40292

Received: August 2, 2004; In Final Form: November 9, 2004

Analysis of the topology of the electron density and underlying local orbital interactions of the fully optimized structure of the molecular cage of the *in*-bicyclo[4.4.4]-1-tetradecyl cation reveals that the inside 3c2e C−H···C hydrogen bond is not only unusual but also strong. The inside C−H bond of the unsaturated, neutral precursor bicyclo[4.4.4]-1-tetradecene is involved in an intramolecular C−H/π interaction with the transannular double bond. Known and calculated ^{1}H and ^{13}C NMR properties, including diamagnetic and paramagnetic contributions to shielding tensors, are accounted for in terms of electron density redistributions and the unusual electronic environment within these hydrocarbon cages.

1. Introduction

Hydrogen bonds involving the C−H group are unusual. The existence of C−H/π, C−H$^+$···C, and C−H/metal agostic bonds, for example, defies the cannon of undergraduate chemistry that a hydrogen bond is a special bridging interaction of a partially positive charged proton situated between two highly electronegative centers (such as N, O, F). The study reported here focused on the electronic nature of a stable, linear C−H···C hydrogen bond in the molecular cage of the *in*-bicyclo[4.4.4]-1-tetradecyl cation,[1−3] denoted herein as C444CH$^+$. This is a transannular hydrogen bond obtained by protonation of the double bond of the inside isomer of bicyclo[4.4.4]-1-tetradecene as shown in the scheme below. The precursor molecule will be denoted herein as C444C.

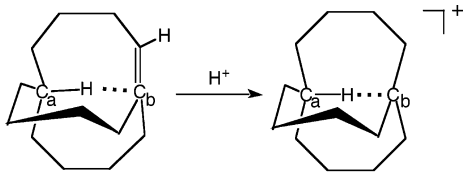

C444C C444CH$^+$

Linearity and close carbon−carbon (C_a···C_b) bridgehead distance is maintained by the constraints of the hydrocarbon cage consisting of three loops, each with a four-carbon backbone. This three-center, two-electron (3c2e) hydrogen bond may be thought of as arising from internal electron density rearrangements that prevent the development of an unstable carbocation center at C_b when the adjacent vinylic carbon is protonated. As we will prove herein, this seemingly electron deficient hydrogen bond, bridging two carbon atoms of low electronegativity, is not only unexpected but is also quite strong with covalent properties. Previously measured ^{1}H and ^{13}C NMR properties of the above two molecules are rationalized in terms of the topology of the electron density about critical nuclei and viewed also in terms of local orbital interactions more familiar to chemists. The analysis was carried out with the use of the theory of atoms in molecules[4−7] (AIM) and localized, natural bond orbital (NBO) theory.[8−10] Molecular geometries and wave functions were calculated with density functional theory. A previous ab initio calculation, including NMR properties of C444CH$^+$, has been reported[11] with somewhat different results.

2. Methods

The equilibrium geometries of the molecules of this study were fully optimized, including normal-mode frequency analysis, using, unless otherwise noted, density functional theory (DFT) at B3LYP/6-31G(d,p), as implemented in Gaussian98.[12] The B3LYP exchange-correlation functional and the use of this polarized basis set have been found to give good results for hydrogen-bonded complexes.[13] ^{1}H and ^{13}C NMR shielding tensors, σ, were obtained with the gauge-independent atomic orbital (GIAO) method.[14,15] The principal components of the tensors were ordered in the convention $\sigma_{11} \leq \sigma_{22} \leq \sigma_{33}$. Chemical shifts were obtained with reference to TMS by using isotropic values of $\sigma_{TMS}(^1H) = 31.76$ ppm and $\sigma_{TMS}(^{13}C) = 191.8$ ppm calculated at the same level of theory. Our calculations included the direction cosines and the diamagnetic and paramagnetic contributions, σ_d and σ_p, respectively, of the isotropic value of $\sigma_{iso} = (\sigma_{11} + \sigma_{22} + \sigma_{33})/3$ of the tensors. Spin−spin couplings, ^nJ(A,B), were also calculated by using routines available in Gaussian03.[16−18]

The resultant electron density obtained from the wave function of all optimized structures was analyzed with AIM.[4,5] NBO theory was also useful in the interpretation of hydrogen bonding in terms of local, hybrid orbital interactions.[8−10]

In the NBO approach, the hydrogen bond is recognized as a general acid/base interaction, with a portion of the lone-pair electron density of the base, n(B), being delocalized into the σ^*(A−H) antibonding orbital of the acidic proton donor.[8−10] In this view n(B)→σ^*(A−H) determines the hydrogen bond. This interaction was assessed quantitatively in this work by use of second-order perturbation theory, where the energy lowering, $E^{(2)}$, due to the interaction of two localized orbitals a and b of energies E_a and E_b, respectively, is given by $E^{(2)} = -2\langle a|\mathbf{F}|b\rangle^2/(E_a - E_b)$, where $\langle a|\mathbf{F}|b\rangle$ is the appropriate element of the one-electron Fock or Kohn−Sham matrix.[9] We prefer the use of NBO theory to other available wave function decomposition schemes[19] due to the direct association of the underlying localized orbitals with concepts (hybrid orbitals, resonance, conjugation, hyperconjugation, charge transfer) familiar to and

* E-mail: d.dupre@louisville.edu.

10.1021/jp046542a CCC: $30.25
Published on Web 01/08/2005

widely used by the chemist. These notions and principles are also put on a quantitative level with NBO theory.

AIM focuses on the true topology of the electron density, obtained either by experiment or by calculation. Here the hydrogen bond is usually found to be a type of closed-shell (as opposed to shared) interaction between the proton donor and the proton acceptor.[4,5,20,21] As in ionic and van der Waals interactions, the electron density at the saddle point, a (3,−1) bond critical point (BCP), along the ridge of maximal density between H and the hydrogen bond acceptor atom is dominantly receding back into the adjacent atomic basins.[4,5] As such, it characteristically has a small value of the electron density, $\rho(r_{cp})$, at the BCP. The Laplacian, which may be written in terms of the eigenvalues of the Hesssian of ρ as $\nabla^2\rho = \lambda_1 + \lambda_2 + \lambda_3$, where $\lambda_1 \leq \lambda_2 \leq \lambda_3$, is also small and positive at this point in a normal hydrogen bond.[4,5,22] The positive sign is due to the dominance ($\lambda_3 > |\lambda_1 + \lambda_2|$) of λ_3, the only positive eigenvalue whose eigenvector at the BCP points along the hydrogen bond path (BP). Covalent bonding, on the other hand, is dominated by contraction of electron density in the plane perpendicular to the bond path at the BCP ($\lambda_3 < |\lambda_1 + \lambda_2|$). The electronic charge is thus concentrated and shared between nuclei. The covalent bond is characterized by large values of $\rho(r_{cp})$ and a large and negative value of $\nabla^2\rho(r_{cp})$. The value of the ratio $|\lambda_1|/\lambda_3$ is also characteristic of the difference between closed shell ($|\lambda_1|/\lambda_3 < 0$) and shared ($|\lambda_1|/\lambda_3 > 0$) bonding patterns.[4,22] The local kinetic energy density per electron, $G(r_{cp})/\rho(r_{cp})$, provides another useful distinction.[22] The potential energy density, $V(r_{cp})$, is locally in excess at the BCP of a shared interaction, and consequently $G(r_{cp})/\rho(r_{cp})$ is small. Due to the retraction of charge density toward the nuclear attractors between juxtaposed atoms in a closed-shell interaction, the kinetic energy dominates and $G(r_{cp})/\rho(r_{cp})$ has a relatively large value and $V(r_{cp})$ is small. The total local energy density $H_b = G(r_{cp}) + V(r_{cp})$, which also reflects the balance between the local kinetic and potential energy densities, is sometimes also quoted as a measure of covalency.[23]

The degree of localization, λ(A), of electrons within the AIM-defined atomic basins and their delocalization, δ(A,B), into the basins of other atoms was also calculated as described by Fradera et al.[24] and Biegler-Konig and Schonbohm.[25] These calculations are based on integrations of the electron-pair density over individual atomic basins and between bonded and non-bonded atomic basins within the molecule. The indices provide a measure of electron-pair sharing arising from exchange correlation by averaging the effect of following the spread of the Fermi hole of a representative electron, which excludes a like amount of density from another same-spin electron. Coulomb correlation is also introduced in our calculations through density functional theory.

3. Results and Discussion

The results of the geometric optimizations for the molecules of this study are shown in Table 1. The intramolecular hydrogen bond of our main attention is denoted C_a−H···C_b. If there is a distinction, the distance of C_a to H is shorter. The bridgehead carbon−carbon distance is seen to considerably contract (by ∼0.5 Å) upon protonation of the C444C precursor. The 3c2e hydrogen bond is linear and the bridgeheads are flattened (the sum of carbon−carbon bond angles about each bridgehead is 348°; perfectly flat would be 360°; exactly tetrahedral, 328.5°). The calculated, unscaled harmonic $\nu(C_a-H)$ stretching frequency is close to that measured by IR spectroscopy.[1] It is noteworthy that the C_a···C_b bridgehead carbon−carbon distance of 2.528 Å in C444CH$^+$ is the same as the N_a···N_b distance in the diamine counterpart,[26−30] inside-protonated 1,6-diazabicyclo-[4.4.4]tetradecane, denoted here as [444]H$^+$. We have previously demonstrated by the methods of this paper that [444]H$^+$ exhibits a strong three-center, *four*-electron (3c4e) hydrogen bond.[26]

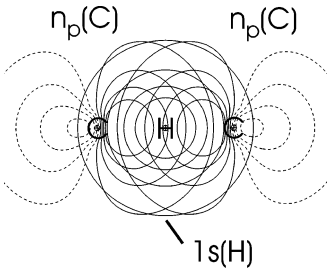

Figure 1. Natural bond orbital representation of the 3c2e hydrogen bond in C444CH$^+$. Two p lone-pair orbitals, n_p(C), located on each bridgehead carbon overlap strongly with the hydrogen 1s orbital. Each n_p(C) orbital is occupied with 0.76 electrons and the 1s(H) orbital contains 0.79 electrons.

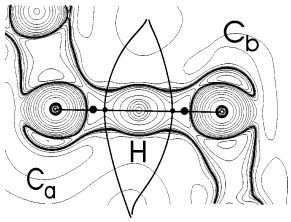

Figure 2. Contour plot of the Laplacian of the electron density showing regions of charge concentration along the almost symmetric C_a−H···C_b hydrogen bond in C444CH$^+$. The lighter lines are areas of charge depletion in the carbon atom cores and extra-valence regions. The vertical curves show where the interatomic surface of H passes through the plane of the figure. The small solid circles on the interatomic surface curves are (3,−1) bond critical points along the bond paths connecting the bridging hydrogen with the nuclear attractors of C_a and C_b. The Laplacian of the electron density reveals that this unusual, enforced hydrogen bond also has substantial covalent character.

TABLE 1: Geometric Parameters and Calculated $\nu(C_a-H)$ Vibrational Stretching Frequencies (in cm^{-1}) for C444CH$^+$ and the C444C Precursor[a]

	C444CH$^+$	C444C
C_a−H	1.262	1.072
C_b···H	1.266	1.980
C_a···C_b	2.528	3.044
∠C_aHC_b	179.8	171.0
sum of bridgehead carbon angles		
C_a	347.6	343.7
C_b	347.7	359.9
$\nu(C_a-H)$	2033.7 (2113)[b]	3318.7

[a] C_a and C_b are the bridgehead carbons. Geometries optimized at B3LYP/6-31G(d,p). Distances in Å; angles in deg. [b] Experimental value from ref 1.

3.1. The 3c2e Hydrogen Bond of C444CH$^+$. NBO theory recognizes the 3c2e hydrogen bond in C444CH$^+$ as the union of two equivalent, lone-pair p-orbitals on each bridgehead carbon with the 1s orbital of the bridging hydrogen. Each lone-pair is occupied with 0.76 electrons and is directed along the C_a−H···C_b axis. As shown in the contour plot of Figure 1, the bridgehead lone pairs, n_p(C), strongly overlap the 1s(H) orbital, itself containing 0.79 electrons. This orbital interaction picture is similar to the three-center molecular orbital interpretation usually given for linear 3c2e bonds.[2,31]

Analysis of the topology of the electron density of this hydrogen bond with AIM gives a similar interpretation, though richer in detail. Figure 2 is a contour plot of the Laplacian, $\nabla^2\rho$, of the electron density ρ in the area of the almost symmetric

TABLE 2: AIM Properties of the 3c2e $C_a-H\cdots C_b$ and 3c4e $N_a-H^+\cdots N_b$ Hydrogen Bonds in Proton Cages $C444CH^+$ and $[444]H^+$ [a]

molecule/bond path	$\rho(r_{cp})$	$\nabla^2\rho(r_{cp})$	λ_1	λ_2	λ_3	$\lvert\lambda_1\rvert/\lambda_3$	ϵ	$G(r_{cp})$	$V(r_{cp})$	H_b	$G(r_{cp})/\rho(r_{cp})$
$C444CH^+$											
C_a-H	0.1551	−0.1945	−0.2898	−0.2897	0.3850	0.75	0.003	0.0529	−0.1545	−0.102	0.341
$C_b\cdots H$	0.1570	−0.2024	−0.2949	−0.2948	0.3874	0.76	0.003	0.0533	−0.1571	−0.104	0.339
C444C											
C_a-H	0.3021	−1.1076	−0.7999	−0.7984	0.4906	1.63	0.002	0.0540	−0.3849	−0.331	0.179
$C_b\cdots H$	0.0322	0.0837	−0.0399	−0.0271	0.1507	0.26	0.475	0.0226	−0.0244	−0.002	0.702
$[444]H^+$											
N_a-H	0.1751	−0.3888	−0.5128	−0.5128	0.6369	0.81	0.000	0.0733	−0.2438	−0.170	0.419
$N_b\cdots H$	0.1753	−0.3904	−0.5137	−0.5137	0.6369	0.81	0.000	0.0733	−0.2442	−0.171	0.418

[a] Data are presented also for the C444C precursor base. The optimized geometry for the diamine analogue, $[444]H^+$, was taken from our previous study [ref 26]. The wave functions for this work were calculated at B3LYP/6-31G(d,p).

$C_a-H\cdots C_b$ hydrogen bond of $C444CH^+$. A continuous region of valence shell charge concentration (within the darker boundary) is clearly seen across the span of the hydrogen bond. Values of the properties of the bond critical points (Table 2) along the bond paths (shown also in Figure 2) between H and the two bridgehead carbons are indicative of significant covalency. The value of $\rho(r_{cp}) = 0.1551$ (0.1570) at each bond critical point is more than half of the value for the shorter and unquestionably covalent C_a-H bond in C444C. Characteristic of a shared interaction,[4,5] $\nabla^2\rho(r_{cp}) = -0.1945$ (−0.2024) is negative at these critical points and about $^1/_5$ of the value recorded for the C_a-H single bond of C444C. The total local energy density, $H_b = G(r_{cp}) + V(r_{cp})$, is also taken as a measure of covalent character in otherwise closed-shell interactions such as the hydrogen bond.[23] Here the local potential energy density $V(r_{cp})$ outweighs kinetic $G(r_{cp})$ contributions and $H_b = -0.102$ (−0.104) is negative and about $^1/_3$ of the value of the reference C_a-H covalent bond in the neutral precursor molecule. The λ_1 and λ_2 eigenvalues are both reflective of the degree of inward curvature of the electron density perpendicular to the bond axis at the bond critical point. The similarity of these values and the corresponding low value of the ellipticities $\epsilon = \lambda_1/\lambda_2 - 1$ is indicative of the cylindrical symmetry of this partially covalent hydrogen bond. These values are close to (though not as large as) those found in our previous study[26] of the diamine proton cage, $[444]H^+$, and reproduced here also in Table 2 (see also the similarities of Figure 2 with Figure 2 of ref 26). The value of the kinetic energy density per electron, $G(r_{cp})/\rho(r_{cp})$, is actually lower in the hydrogen bond paths of the carbon proton cage than for the diamine analogue. This is reflected in the lesser, relative contraction of charge into the bridgehead basins in $C444CH^+$, given by the values of the $|\lambda_1|/\lambda_3$ ratio, also listed in Table 2.

A question arises at this point as to how the three-center bond of $C444CH^+$, with nominally only two valence electrons, can have an intramolecular hydrogen bond of strength rivaling that of $[444]H^+$, with nominally four bonding electrons. This apparent inconsistency is reconciled by looking at the *redistribution* of charge around the molecular frame that serves to delocalize the positive charge of the carbocation that emerged upon protonation of the double bond of C444C. Inspection of the AIM charges of Table 3 shows that both bridgehead carbons of $C444CH^+$ are approximately *neutral* (+0.02). The carbon atoms in the four hydrocarbon loops are positive (atomic charges between 0.11 and 0.12), as are many of the methylene hydrogen atoms (charges not listed). Electron density has been lost from the latter atoms and transferred to the hydrogen bond to avoid the creation of an unstable carbocation center at C_b. In the process, the bridging μ-hydrido proton was left with a small *negative* charge (−0.05). This mechanism is also recovered in AIM localization and delocalization indices, shown in Table 3

TABLE 3: AIM Charges and Localization, λ(A), and Delocalization, δ(A,B), Indices Across the Hydrogen Bond and One Representative Hydrocarbon Loop of the $C444CH^+$ Proton Cage (3c2e Hydrogen Bond)[a]

$C444CH^+$	C_a	αC	βC	γC	δC	C_b	H
AIM charge	0.02	0.11	0.11	0.12	0.10	0.02	−0.05
λ(A)	3.91	3.83	3.83	3.82	3.84	3.90	0.43
δ(A,B)							
C_a with ...		0.96	0.04	0.01	0.02	0.15	0.49
H with ...	0.49	0.03	0.01	0.01	0.03	0.49	
$[444]H^+$	N_a	αC	βC	γC	δC	N_b	H
AIM charge	−0.98	0.39	0.11	0.10	0.38	−0.98	0.50
λ(A)	6.05	3.63	3.83	3.83	3.63	6.05	0.10
δ(A,B)							
N_a with ...		0.87	0.06	0.01	0.00	0.16	0.35
H with ...	0.35	0.01	0.00	0.00	0.01	0.35	

[a] Data obtained from a previous study of the 3c4e hydrogen bond in the diamine proton cage analogue, $[444]H^+$, are included for comparison, see ref 26. Geometries optimized at B3LYP/6-31G(d,p), except for $[444]H^+$ (symmetric, low barrier transition state), which was optimized from ref 26 at the B3LYP/6-31G+(d,p) level. AIM data obtained from wave functions at B3LYP/6-31G(d,p). A representative hydrocarbon loop between bridgehead carbons (C_a,C_b) or nitrogens (N_a,N_b) is indicated by −αC−βC−γC−δC−; the hydrogen bonded proton, by H.

for the atoms of the hydrogen bond and around a representative hydrocarbon loop (denoted $-\alpha CH_2-\beta CH_2-\gamma CH_2-\delta CH_2-$). As befits the lower positive (more negative) charge, the electron pair localization index of the bridgehead carbons is greater than that of the methylene carbons. The delocalization index between the α-carbons and the bridgeheads is large at 0.96. Counting the equivalent δ-carbons, there are six of these interactions, resulting in a buildup of electron pair density at C_a and C_b that spills over into the atomic basin of H.

On the average, the atomic basin of H contains 1.05 electrons. Of these, 0.43 are localized within the basin and are not shared with other atoms. From the delocalization indices, 0.49 electrons are shared with each of the two bridgehead carbon atoms. There is some small additional sharing of electron density of the H atom with other atomic basins in the molecule, most notably the α- and δ-carbons. Since the C−H bonds are essentially nonpolar, this $C_a-H\cdots C_b$ hydrogen bond may be interpreted as being mainly due to equal sharing of approximately half of an electron pair between the H atom and each of the bridgehead carbons. (In methane the delocalization index across the C−H bond is 0.98, meaning here that approximately one electron pair is shared in the covalent single bond between what are also essentially neutral carbon and hydrogen atoms.[24]) Noteworthy also in $C444CH^+$ is the joint delocalization index of 0.15 between the two bridgehead carbons, indicating communication between these atoms across the hydrogen bond. The slightly

negative, almost neutral, charge on H also has consequences in shielding of the proton. A signature feature of 3c2e hydrogen bonds is a large *upfield*, even negative value of ^{1}H NMR chemical shifts. Characteristics of nuclear shielding tensors of atoms involved in this hydrogen bond will be discussed more fully in section 3.3 below. We note here that the earlier Hartree−Fock, ab initio study of Cioslowski[11] resulted in a stronger AIM derived negative charge (−0.23 vs our −0.05) of the bridging proton of C444CH$^+$ and thus severely overestimated the negative value of $\delta(^1\text{H})$ for this hydrogen atom. We find in our calculations that the atoms of the C_a−H···C_b bond are essentially neutral and the two carbon−hydrogen bonds are nonpolar.

The bonding pattern of the 3c2e H-bond of C444CH$^+$ is very similar to that of the diamine analogue. There are, however, some distinctions. In the 3c4e hydrogen bond of [444]H$^+$, the bridgeheads are two more electronegative, nitrogen atoms. Charge is given up to these nitrogens, particularly by the bridging proton and the nearest neighbor α (and equivalent δ) carbons. These atomic sites are seen to have lower localization indices in [444]H$^+$ than in the C444CH$^+$ cage. Although the delocalization index of each nitrogen to the methylene carbons around the loops is similar to those found with carbon bridgeheads, electron pair localization on the negatively charged nitrogens is high (6.05) and the bridgeheads are negatively charged (−0.98). The bridging H atom in [444]H$^+$ is positively charged (0.50) and, therefore, has fewer electrons to share in the hydrogen bond. The localization index of H of these 0.50 electrons is only 0.10 and its delocalization index with each nitrogen basin is only 0.35. The delocalization index of H into atoms other than the neighboring nitrogens is minuscule. As pointed out by Fradera et al.,[24] it would not be correct to interpret the value of 0.35 as representing only approximately $^1/_3$ of an electron-pair being shared between the H atom and each nitrogen. The smaller delocalization index across the polar bonds of N_a−H$^+$···N_b, however, is indicative of unequal sharing of electron pair density pulled more into the domain of the electronegative nitrogen attractors. The extension of the nitrogen basins due to charge transfer from H is also evident in the positions of the bond critical points along the respective bond paths. The bond critical points of each N−H$^+$ bond path are only 0.334 Å from the bridging proton (26% along the BP from the proton to each respective nitrogen nucleus), whereas those for the C−H bonds in C_a−H···C_b are 0.522 Å away, almost halfway between the carbon and hydrogen nuclei (41% along the BP from the proton to respective carbon nuclei). Finally, the positive charge on the H atom in [444]H$^+$ results in a strong downfield ^{1}H NMR chemical shift of $\delta(^1\text{H}) = 17.4$.[30]

3.2. An Intramolecular C−H/π Interaction in the C444C Precursor. The C444CH$^+$ molecule of this study is somewhat unusual for proton cages in that the emerging, formally positive H$^+$ atom is already inside the framework in the neutral precursor molecule, C444C. So also is one face of the π-electron density of the double bond at the C_b bridgehead. NBO calculations reveal a π(C═C) interaction of this double bond with the σ^*(C_a−H) antibond and the 2s Rydberg orbital of the H atom. The π(C═C) → σ^*(C_a−H) interaction has second-order perturbation energy $E^{(2)}$ of 5.63 kcal/mol and the π(C═C) → Ryd*(2s) interaction is measured by $E^{(2)} = 1.19$ kcal/mol. An illustration of the extensive local orbital overlap of the first case is given in Figure 3. Although the internal C_a−H bond points closer to the bridgehead carbon than the center of the double bond, the AIM bond path between H and C_b is highly curved and bowed toward the bond critical point of C═C, as shown in Figure 4. A conflict catastrophe,[4] similar to that found in hydrogen halides[32−34] and water[35,36] loosely bound to ethylene, appears to be frustrated by geometric constraints within the carbon cage. The parameters (Table 2) of the bond critical point between H and C_b are characteristic of a weak hydrogen bond: $\rho(r_{cp}) = 0.0322$ is small, $\nabla^2\rho(r_{cp}) = 0.0837$ is small and positive (closed-shell interaction), $H_b = -0.002$ is only slightly negative, and the local kinetic energy density per electron, $G(r_{cp})/\rho(r_{cp}) = 0.702$, is large. The eigenvalues λ_1 and λ_2 are also substantially different and, befitting the asymmetry of the inside of this unsaturated hydrocarbon cage, produce an ellipticity, ϵ, at the bond critical point of 0.475.

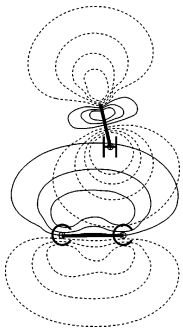

Figure 3. Natural bond orbital overlap showing the substantial π(C═C) → σ^*(C_a−H) interaction in the interior of the C444C hydrocarbon cage. The C_a bridgehead carbon is out of the plane of the figure which contains the double bond (>C═C<) and the inside hydrogen, H.

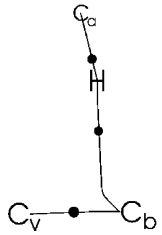

Figure 4. Molecular graph of the C_a−H/π interaction in the interior of C444C. The solid circles are (3,−1) bond critical points along the bond paths connecting the nuclear attractors. C_a (out-of-plane) and C_b are the bridgehead carbons, C_v is the vinylic carbon, and H is the inside hydrogen. The curved path between H and C_b indicates a frustrated conflict catastrophe involving the double bond of >C_b═C_v<.

TABLE 4: Calculated and Experimental NMR Chemical Shift and *J*-Coupling Data for C444CH$^+$ [a]

	δ (ppm)	
C444CH$^+$ atom	exptl[b]	calcd
H	−3.46	−3.90
C_a, C_b	139.3	141.7, 139.7
αC	41.6	42.1, 42.2
βC	19.3	19.6, 19.7
(αC)H	2.5	3.14, 2.07
(βC)H	1.9	1.86, 2.05
$^1J(C_a,H)$, $^1J(C_b,H)$ (Hz)	47	44.9, 45.8
$^{2h}J(C_a,C_b)$ (Hz)		12.4

[a] The calculations were performed with the GIAO method at the B3LYP/6-31G(d,p) level. αC and βC denote the nearest and next nearest neighboring carbons, respectively, to either bridgehead carbon C_a or C_b. (αC)H and (βC)H indicate the proton attached to carbons αC and βC. [b] Experimental value from ref 3.

3.3. ^{1}H and ^{13}C NMR Chemical Shifts and Shielding Tensors. The results of our NMR calculations for selected carbon and hydrogen atoms of C444C and C444CH$^+$ are presented in Tables 4 and 5. It has been shown recently[37] that effects of electron correlation on theoretical values of ^{1}H NMR chemical shifts, though small for normal hydrogen bonds, should not be neglected in the study of strong hydrogen bonds. We

TABLE 5: Calculated and Experimental NMR Chemical Shift and *J*-Coupling Data for C444C[a]

	δ (ppm)	
C444C atom	exptl[b]	calcd[c]
C_a		29.4
C_b	143.0	148.0
C_v	131.7	130.2
H	3.35	4.26
H_v	5.42	5.86
$^1J(C_a,H)$ (Hz)		118.9
$^1J(C_v,H_v)$ (Hz)	143.5	137.7

[a] The calculations were performed with the GIAO method at the B3LYP/6-31G(d,p) level. C_a and C_b are the bridgehead carbons. The *in*-C_a−H bond points toward the C_b═C_v double bond, where C_v denotes the vinylic carbon, also bonded to the outside vinylic hydrogen, H_v. [b] Experimental value from ref 1. [c] Calculations show that H is in a more anisotropic electronic environment within the cage, with $\sigma_{iso}(H) = 27.5$ and $\Delta\sigma(H) = \sigma_{||} - \sigma_{\perp} = 15.12$. As a comparison $\sigma_{iso}(H_v) = 25.9$, but $\Delta\sigma(H_v)$ is only 6.31.

find that the use of the B3LYP hybrid functional along with the 6-31G(d,p) basis set does a good, and computationally economical, job in reproducing the available ^{13}C and ^1H NMR experimental data for these molecules. We have also calculated the shielding tensor components, listed in Table 6, and examined their orientation in the molecular frame. No experimental information on shielding tensor components appears to be available for the nuclei of atoms in these compounds.

^1H NMR is sensitive to the nature and strength of hydrogen bonding. Proton chemical shifts are found further downfield from TMS when a hydrogen atom is engaged in hydrogen bonding. In strong hydrogen bonds, $\delta(^1H)$ can even be in the range of 14−22 ppm.[38] Contrary to the situation in the more common 3c4e hydrogen bonds, however, the signature of 3c2e hydrogen bonding is a large *upfield* shift with *negative* values of $\delta(^1H)$.[1−3] An understanding of the causes of these differences is available from analysis of orbital and topological features of the electron density across the respective hydrogen bonds.

In his early study of the water dimer, Ditchfield[39] recognized that the deshielding of the donor proton upon hydrogen bond formation is a result of two factors. First, there is loss of electron density about the proton, arising from elongation of the O−H donor bond and charge transfer. We would also note for this factor that charge is transferred from the proton acceptor molecule into the proton donor molecule. In NBO terms, an intermolecular n(O) → σ^*(O−H) interaction takes place in the water dimer. In addition to weakening the donor O−H bond, electron density repolarizations occur that serve to change the charge on atoms of both molecules. Second, deshielding currents arising from the heavier atom of the impinging acceptor site were shown to be more important than previously thought and produce anisotropic paramagnetic effects along the axis of the hydrogen bond. Ditchfield[39] proposed that the increase of the anisotropy of the shielding tensor upon hydrogen bond formation should be more revealing of the nature of the hydrogen bond than the averaged $\sigma_{iso}(^1H)$ value. The shielding anisotropy will be defined here as $\Delta\sigma = \sigma_{||} - \sigma_{\perp}$, where $\sigma_{||}$ is the component of the tensor parallel to axis of the hydrogen bond and $\sigma_{\perp}$ is the average of the two perpendicular components.

We have found Ditchfield's hypothesis to be true in a weaker three-center, *four*-electron (3c4e) C−H^+···C bond formed in the proton-bound dimer of Arduengo's stable, singlet-carbene, 1,3-dimethylimidazol-2-ylidene.[40] As shown below, the shielding tensor of the proton in the hydrogen bond is oriented with its major σ_{33}-axis along the almost linear C−H^+···C axis of the dimer. As seen from the data in Table 6, $\sigma_{iso}(^1H)$ falls from 24.04 ppm in the monomeric imidazolium cation to 16.48 ppm upon the formation of the hydrogen bond. The anisotropy $\Delta\sigma = \sigma_{||} - \sigma_{\perp}$ of the tensor, however, *increases* from 1.85 to 17.67 ppm. The diamagnetic components $\sigma_d(^1H)$ of the tensors are about the same, with $\sigma_d(^1H) = 31.56$ and 33.17 ppm before and after dimerization, respectively. Since the imidazolium C_a−H^+ bond is elongated in the hydrogen bond, this increase in diamagnetic shielding is indicative of some accumulation of s-electron density on the proton due to charge transfer from the in-plane lone pair of the singlet carbene. Accompanying the above is a dramatic change in the $\sigma_p(^1H)$ paramagnetic components, with $\sigma_p(^1H) = -7.53$ ppm before and −16.69 ppm after the hydrogen bond develops. The latter effect is due to induced currents arising from the carbon lone pair on the carbene monomer fragment in the complex and is most important in the deshielding of the proton in the hydrogen-bonded dimer.

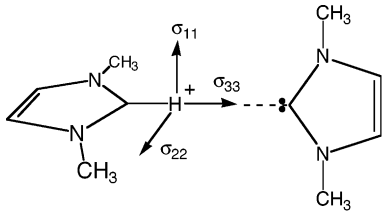

bis(1,3-dimethyl)imidazol-2-ylidene proton complex

The situation in the 3c2e, intramolecular hydrogen bond of this study is, however, very different. Here, as a result of internal electron redistribution discussed in section 3.1 above and despite the elongation of the C_a−H bond, the electron density in the atomic basin of the inside proton changes little upon protonation of C444C. (AIM charge on H goes from 0.01 to −0.05.) As seen in the data listed in Table 6, $\sigma_{iso}(^1H)$ of this proton rises from 27.47 ppm in the precursor to 35.66 ppm in C444CH^+. This results on the δ-scale in a negative value of the chemical

TABLE 6: NMR Shielding Tensors for the Hydrogen-Bonded Proton in C444CH^+ and the C_a−H and Vinylic H_v Protons in the C444C Neutral Precursor[a]

H atom[b]	σ_{11}	σ_{22}	σ_{33}	σ_{iso}	$\Delta\sigma = \sigma_{||} - \sigma_{\perp}$	σ_d	σ_p
proton cages							
C444CH^+	33.41	33.46	40.10	35.66	6.67	40.28	−4.63
C444C: inside H	20.35	24.50	37.55	27.47	15.12	37.43	−9.97
C444C: vinylic H_v	21.44	26.11	30.09	25.88	6.31	35.13	−9.24
carbene dimer							
1,3-dimethylimidazol-2-ylidene	8.50	12.68	28.26	16.48	17.67	33.17	−16.69
imidazolium monomer	20.45	25.27	26.39	24.04	1.85	31.56	−7.53

[a] Also shown for comparison are similar data for the 3c4e C−H^+···C hydrogen bond in a proton-bound carbene dimer 1,3-dimethylimidazol-2-ylidene and the imidazolium monomer cation. Tensor principal components are ordered in the convention $\sigma_{11} \le \sigma_{22} \le \sigma_{33}$ and the anisotropy $\Delta\sigma = \sigma_{||} - \sigma_{\perp}$, is defined parallel and perpendicular to the C−H axis. σ_d and σ_p are the isotropic diamagnetic and paramagnetic contributions, respectively, to σ_{iso}. Calculations performed with the GIAO method using B3LYP/6-31G(d,p). [b] Hydrogen bonded proton unless otherwise indicated.

shift, $\delta(^1H) = -3.90$. The experimental value (Table 4) is −3.46 ppm.[1−3] Proton shielding is also reflected in the increase of the diamagnetic component of the tensor, with $\sigma_d(^1H)$ going from 37.43 ppm in C444C to 40.28 ppm in the hydrogen bond. More significantly, the paramagnetic component increases (decreases in absolute value) from $\sigma_p(^1H) = -9.97$ to −4.63 ppm. Thus, the anisotropy $\Delta\sigma = \sigma_{||} - \sigma_{\perp}$ is larger before hydrogen bond formation: 15.12 ppm vs 6.67 ppm. This unusual feature can be traced to the anisotropic currents of the double bond present in the C−H/π interaction in C444C as described above in section 3.2. In both C444C and C444CH$^+$, the largest σ_{33} component of the shielding tensor points along the C_a−H axis. The perpendicular components σ_{11} and σ_{22} are almost the same and closer to the value of σ_{33} in the very symmetric hydrogen bond of C444CH$^+$. The anisotropy of the $\sigma(^1H)$ shielding tensor is thus lower in C444CH$^+$.

Experimental NMR information (Table 5) is also available for some of the important atoms of C444C, including the vinylic carbon, C_v, and its bound hydrogen, H_v. The inside hydrogen is more shielded than H_v by about 2 ppm. The ^{13}C NMR chemical shift of the bridgehead carbon C_b of C444C is significantly downfield from C_v even though both carbons participate in the double bond and are approximately sp^2 hybridized. The C_b bridgehead is flat with the sum of bridgehead carbon−carbon bond angles equal to 359.9°. The double bond of our theoretical model, however, is found to be slightly twisted out-of-plane and the atoms connected to C_v are somewhat distorted from planarity. The other bridgehead carbon, C_a, bound to the inside proton is pyramidalized (sum of bridgehead carbon−carbon bond angles, 343.7°) and hence more sp^3 hybridized. This nucleus has a small calculated $\delta(^{13}C_a)$ of 29.4 ppm. We note that there are some unassigned ^{13}C NMR chemical shifts in this area for this compound reported in the Experimental Section of ref 1.

^1J(C,H) couplings have also been measured[1] for the bridgehead carbons of C444C and C444CH$^+$ and are listed in Tables 4 and 5, respectively. Our calculated value for $^1J(C_a,H) = 44.9$ Hz and $^1J(C_b,H) = 45.8$ Hz in the C444CH$^+$ model compares well with the experimental value of 47.0 Hz. Our calculated value of $^{2h}J(C_a,C_b) = 12.4$ Hz could be of use in future studies, using isotopic enrichment, of communication of bridgehead carbons through bonds straight across the cage. This effect was noted in section 3.1 above in the AIM delocalization index between carbons C_a and C_b, and would be further experimental evidence of an electron-mediated connection between these atoms across the hydrogen bond. Similar effects have recently been found experimentally for other traditional hydrogen bonds in proteins and nuclei acids.[41−45] $^1J(C_v,H_v) = 143.5$ Hz has been reported for the vinylic C−H bond in C444C. Our calculated value is 137.7 Hz. The $^1J(C_a,H)$ coupling constant apparently has not been measured for this compound. Our prediction would be a value around 118.9 Hz.

4. Conclusions

The unusual, enforced C−H···C hydrogen bond in C444CH$^+$ is stronger than previously recognized and has covalent character. Charge redistribution occurs after protonation of the double bond of the C444C precursor compound so as to prevent the development of an unstable, bridgehead carbocation. Consequently, the formally 3c2e hydrogen bond of C444CH$^+$ has topological properties similar to those found for the 3c4e diamine analogue, which we have previously shown[26] to have covalent character in isolation. The precursor compound C444C exhibits an intramolecular, inside C−H/π interaction[46] with topological properties close to a conflict catastrophe.

The signature, upfield and negative ^1H NMR chemical shift of this 3c2e hydrogen bond is shown to be due to the above-mentioned electron delocalization that produces nearly neutral atoms across C_a−H···C_b. Even though bonded to two other carbons, the bridging H atom is thus essentially in the 1s^1 electronic configuration and the proton is highly shielded. The AIM delocalization index of the connecting H atomic basin shows that, on the average, the approximate single electron pair shared in a covalent single C−H bond (as in CH_4 for example) is split equally between the atomic basins of the bridging carbons in C444CH$^+$.

Most of the ^1H and ^{13}C NMR properties calculated with the B3LYP hybrid functional and the 6-31G(d,p) basis set are in good agreement with experimental values where known. The bridgehead carbons of C444CH$^+$ communicate with one another through the hydrogen bond, with a predicted $^{2h}J(C_a,C_b)$ of 12.4 Hz and an AIM delocalization index of 0.15.

Changes in the anisotropy of the ^1H shielding tensor in the formation of the 3c2e hydrogen bond of C444CH$^+$ are opposite to that predicted by Ditchfield[39] for normal hydrogen bonds and to that calculated and reported here for the 3c4e C−H$^+$···C hydrogen bond of a stable, proton-bound carbene dimer. These results can be explained in terms of the very different electronic environment near C_a−H before (C−H/π interaction) and after protonation (nearly symmetric hydrogen bond) of the C444C precursor.

Acknowledgment. Supercomputer time allocations received from the National Computational Science Alliance and from the Advanced Biomedical Computing Center of the Frederick Cancer Research and Development Center, National Institutes of Health are acknowledged. Support for this work also came from a Research Initiation Grant from the Office of the Vice President for Research, University of Louisville. Helpful discussions with Dr. Eduard Chekmenev are also acknowledged.

References and Notes

(1) McMurry, J. E.; Lectka, T.; Hodge, C. N. *J. Am. Chem. Soc.* **1989**, *111*, 8867.
(2) McMurry, J. E.; Lectka, T. *J. Am. Chem. Soc.* **1993**, *115*, 10167.
(3) McMurry, J. E.; Lectka, T. *Acc. Chem. Res.* **1992**, *25*, 47.
(4) Bader, R. F. W. *Atoms in molecules. A quantum theory*; Clarendon Press: Oxford, UK, 1990.
(5) Popelier, P. *Atoms in molecules. An introduction*; Prentice Hall: New York, 2000.
(6) Bader, R. F. W.; MacDougall, P. J.; Lau, C. D. H. *J. Am. Chem. Soc.* **1984**, *106*, 1594.
(7) Bader, R. F. W. *J. Phys. Chem.* A **1998**, *102*, 7314.
(8) Reed, A. E.; Curtiss L. A.; Weinhold, F. *Chem. Rev.* **1988**, *88*, 899.
(9) Weinhold, F. Natural Bond Orbital Methods. In *The Encyclopedia of Computational Chemistry*; Schleyer, P. v. R., Editor-in-Chief; John Wiley & Sons: Chichester, UK, 1998.
(10) Reed, A. E.; Weinhold, F.; Curtiss, L. A.; Pochatko, D. J. *J. Chem. Phys.* **1986**, *84*, 5687.
(11) Cioslowski, J. *J. Am. Chem. Soc.* **1993**, *115*, 5177.
(12) Frisch, M. J.; Trucks, G. W.; Schlegel, H. B.; Scuseria, G. E.; Robb, M. A.; Cheeseman, J. R.; Zakrzewski, V. G.; Montgomery, J. A., Jr.; Stratmann, R. E.; Burant, J. C.; Dapprich, S.; Millam, J. M.; Daniels, A. D.; Kudin, K. N.; Strain, M. C.; Farkas, O.; Tomasi, J.; Barone, V.; Cossi, M.; Cammi, R.; Mennucci, B.; Pomelli, C.; Adamo, C.; Clifford, S.; Ochterski, J.; Petersson, G. A.; Ayala, P. Y.; Cui, Q.; Morokuma, K.; Salvador, P. J.; Dannenberg, J.; Malick, D. K.; Rabuck, A. D.; Raghavachari, K.; Foresman, J. B.; Cioslowski, J.; Ortiz, J. V.; Baboul, A. G.; Stefanov, B. B.; Liu, G.; Liashenko, A.; Piskorz, P.; Komaromi, I.; Gomperts, R.; Martin, R. L.; Fox, D. J.; Keith, T.; Al-Laham, M. A.; Peng, C. Y.; Nanayakkara, A.; Challacombe, M.; Gill, P. M. W.; Johnson, B.; Chen, W.; Wong, M. W.; Andres, J. L.; Gonzalez, C.; Head-Gordon, M.; Replogle, E. S.; Pople, J. A. *Gaussian 98*, Revision A.11; Gaussian, Inc.: Pittsburgh, PA, 2001.
(13) Del Bene, J. E.; Person, W. B.; Szczepaniak, K. *J. Phys. Chem.* **1995**, *99*, 10705.

(14) Wolinski, K.; Hinton, J. F.; Pulay, P. *J. Am. Chem. Soc.* **1990**, *112*, 8251.
(15) Cheeseman, J. R.; Trucks, G. W.; Keith, T. A.; Frisch, M. J. *J. Chem. Phys.* **1996**, *104*, 5497.
(16) Frisch, M. J.; Trucks, G. W.; Schlegel, H. B.; Scuseria, G. E.; Robb, M. A.; Cheeseman, J. R.; Montgomery, J. A., Jr.; Vreven, T.; Kudin, K. N.; Burant, J. C.; Millam, J. M.; Iyengar, S. S.; Tomasi, J.; Barone, V.; Mennucci, B.; Cossi, M.; Scalmani, G.; Rega, N.; Petersson, G. A.; Nakatsuji, H.; Hada, M.; Ehara, M.; Toyota, K.; Fukuda, R.; Hasegawa, J.; Ishida, M.; Nakajima, T.; Honda, Y.; Kitao, O.; Nakai, H.; Klene, M.; Li, X.; Knox, J. E.; Hratchian, H. P.; Cross, J. B.; Adamo, C.; Jaramillo, J.; Gomperts, R.; Stratmann, R. E.; Yazyev, O.; Austin, A. J.; Cammi, R.; Pomelli, C.; Ochterski, J. W.; Ayala, P. Y.; Morokuma, K.; Voth, G. A.; Salvador, P.; Dannenberg, J. J.; Zakrzewski, V. G.; Dapprich, S.; Daniels, A. D.; Strain, M. C.; Farkas, O.; Malick, D. K.; Rabuck, A. D.; Raghavachari, K.; Foresman, J. B.; Ortiz, J. V.; Cui, Q.; Baboul, A. G.; Clifford, S.; Cioslowski, J.; Stefanov, B. B.; Liu, G.; Liashenko, A.; Piskorz, P.; Komaromi, I.; Martin, R. L.; Fox, D. J.; Keith, T.; Al-Laham, M. A.; Peng, C. Y.; Nanayakkara, A.; Challacombe, M.; Gill, P. M. W.; Johnson, B.; Chen, W.; Wong, M. W.; Gonzalez, C.; Pople, J. A.; *Gaussian 03*, Revision A.1; Gaussian, Inc.: Pittsburgh, PA, 2003.
(17) Sychrovsky, V.; Grafenstein, J.; Cremer, D. *J. Chem. Phys.* **2000**, *113*, 3530.
(18) Helgaker, T.; Watson, M.; Handy, N. C. *J. Chem. Phys.* **2000**, *113*, 9402.
(19) Kitaura, K.; Morokuma, K. *Int. J. Quantum Chem.* **1976**, *10*, 325.
(20) Carroll, M. T.; Chang, C.; Bader, R. F. W. *Mol. Phys.* **1988**, *63*, 387.
(21) Koch, U.; Popelier, P. L. A. *J. Phys. Chem.* **1995**, *99*, 9747.
(22) Bader, R. F. W.; Essén, H. *J. Chem. Phys.* **1984**, *80*, 1943.
(23) Jenkins, S.; Morrison, I. *Chem. Phys. Lett.* **2000**, *317*, 97.
(24) Fradera, X.; Austen, M. A.; Bader, R. F. W. *J. Phys. Chem. A* **1999**, *103*, 304.
(25) Biegler-Konig, F.; Schonbohm, J. *J. Compt. Chem.* **2002**, *23*, 1489.
(26) DuPré, D. B. *J. Phys. Chem. A* **2003**, *107*, 10142.
(27) Alder, R. W.; Orpen, A. G.; Sessions, R. B. *J. Chem. Soc., Chem. Commun.* **1983**, 999.
(28) Alder, R. W.; Eastman, P.; Hext, N. M.; Moss, R. E.; Orpen, A. G.; White, J. M. *J. Chem. Soc., Chem. Commun.* **1988**, 1528.
(29) Alder, R. W.; Moss, R. E.; Sessions, R. R. *J. Chem. Soc., Chem. Commun.* **1983**, 997.
(30) Alder, R. W.; Casson, A.; Sessions, R. B. *J. Am. Chem. Soc.* **1979**, *101*, 3652.
(31) DeKock, R. L.; Bosma, W. B. *J. Chem. Educ.* **1988**, *65*, 194.
(32) Novoa, J. J.; Mota, F. *Chem. Phys. Lett.* **2000**, *318*, 345.
(33) Zhang, Y. H.; Hao, J. K.; Wang, X.; Zhou, W.; Tang, T. H. *J. Mol. Struct. THEOCHEM* **1998**, *455*, 85.
(34) Rozas, I.; Alkorta, I.; Elguero, J. *J. Phys. Chem. A* **1997**, *101*, 9457.
(35) Lin, Z.; Bytheway, I. *Chem. Phys. Lett.* **1995**, *240*, 541.
(36) Vorobyov, I.; Yappert, M. C.; DuPré, D. B. *J. Phys. Chem. A* **2002**, *106*, 10691.
(37) Barich, D. H.; Nicholas, J. B.; Haw, J. F. *J. Phys. Chem. A* **2001**, *105*, 4708.
(38) Jeffrey, G. A. *An Introduction to Hydrogen Bonding*; Oxford University Press: New York, 1997.
(39) Ditchfield, R. *J. Chem. Phys.* **1976**, *65*, 3123.
(40) Arduengo, A. J., III; Gamper, S. F.; Tamm, M.; Calabrese, F. C.; Davidson, F.; Craig, H. A. *J. Am. Chem. Soc.* **1995**, *117*, 572.
(41) Dingley, A. J.; Grzesiek, S. *J. Am. Chem. Soc.* **1998**, *120*, 8293.
(42) Pervushin, K.; Ono, A.; Fernandez, C.; Szyperski, T.; Kainosho, M.; Wuthrich, K. *Proc. Natl. Acad. Sci. U.S.A.* **1998,** *95*, 14147.
(43) Cordier, F.; Grzesiek, S. *J. Am. Chem. Soc.* **1999**, *121*, 1601.
(44) Scheurer, G.; Bruschweiler, R. *J. Am. Chem. Soc.* **1999**, *121*, 8661.
(45) Cornilescu, G.; Ramirez, B. E.; Frank, M. K.; Clore, G. M.; Gronenborn, A. M.; Bax, A. *J. Am. Chem. Soc.* **1999**, *121*, 6275.
(46) Desiraju, G. R.; Steiner, T. *The weak hydrogen bond in structural chemistry and biology;* Oxford University Press: New York, 1999.